Highly Bright and Compact Alloyed Quantum Rods with Near Infrared Emitting: a Potential Multifunctional Nanoplatform for Multimodal Imaging In Vivo

*Duyang Gao, Pengfei Zhang, Zonghai Sheng, Dehong Hu, Ping Gong, Chi Chen, Qian Wan, Guanhui Gao, and Lintao Cai**

Controlling synthesis of near-infrared emitting quantum rods (QRs) for in vivo imaging is a major challenge in the fabrication of multifunctional nanoprobes. Here, a reliable synthetic approach for $CdTe_xSe_{1-x}$/ZnS alloy nanocrystals to achieve highly bright (quantum yields up to 80%) with controllable rod-shape and near-infrared (650–870 nm) emission is developed. Aspect ratio and emission of QRs are correlated with composition, which can be easily tuned by changing Te and Se mole ratio. It illustrates that the content of Se plays an important role in maintaining the rod-shape, while Te has a significant impact on emitting of the nanorods. Besides exhibiting great stability over a broad range of pH (4–10) and ion strength (up to 2 mol L^{-1} NaCl solution), these hydrophilic QRs display good photo stability and storage stability. In particular, the specially absorbing of paramagnetic gadolinium ions on the QRs lead to a versatile method to engineer multimodal imaging nanoprobes, which are applied for in vivo lymph node dual-modal imaging (fluorescence and magnetic resonance imaging). These results suggest a promising strategy for engineering multifunctional imaging nanoprobes with the stable near-infrared QRs.

1. Introduction

Semiconductor nanocrystals (NCs) have emerged as an important class of nanomaterials because of their tunable optoelectronic properties that arise from size, shape and composition. They are used as active components in functional nanocomposites,[1] chemical sensors,[2] biomedicine,[3] and optoelectronics.[4] More recently, the rod architecture also known as quantum rod (QR defined as aspect ratio < 20) has been achieved.[5] Such QRs display the transition from zero-dimensional quantum dots (QDs) to one-dimensional quantum wires (aspect ratio ≥ 20) in the sense that the length becomes a weakly confined axis.[6] They have shown several advantages over spherical NCs for serving as novel materials due to their larger absorption cross section,[7] faster radiative decay rate,[8] bigger Stokes shift[9] and larger surface areas, which facilitate functionalization with multiple binding moieties.[10] There have been many demonstrations of their use for biological imaging, ranging from single molecule tracking to in vivo imaging.[11] The vast majority of these applications have used CdSe-based QRs.[11] It can be attributed in part to the progress of their synthesis and particularly in the growth of CdS, ZnS, or multilayer inorganic shells around CdSe cores to increase their quantum yield (QY) and photo resistance by passivating their surface to avoid oxidation and the charges effects from the surrounding environment.[12] However, with bulk bandgap of 1.74 eV, CdSe QRs are mainly of interest for applications involving only visible light (400–650 nm), which have limited penetration depth in living tissue compared to near-infrared (NIR) fluorophor.[13] Additionally, synthesis of NIR emitting QRs has proved much more challenging and there has not yet been yielded NIR QRs with QY and photo resistance comparable to their CdSe counterparts. Since the optical properties of alloys vary with composition, it is possible to tune the spectrum while maintaining morphology. Thus, it offers an opportunity in selecting desirable properties for nanoscale engineering. To employ alloy NCs using CdSe QRs as scaffold would solve above obstacles. It has been proved by Nie and co-workers, who have prepared CdSeTe alloy QDs achieving continuous tunable optical properties without changing the spherical particle size.[14] CdSeS alloy QDs have been also synthesized successfully by Rosenthal group.[15] However, very little effort has been made to explore the CdSe-based alloy QRs.

Most high-quality NCs are synthesized based on high temperature reaction of organometallic compounds in nonpolar

D. Y. Gao, P. F. Zhang, Dr. Z. H. Sheng, D. H. Hu, Dr. P. Gong, C. Chen, Dr. G. H. Gao, Prof. L. T. Cai
CAS Key Laboratory of Health Informatics
Guangdong Key Laboratory of Nanomedicine
Shenzhen Key Laboratory of Cancer Nanotechnology
Institute of Biomedicine and Biotechnology
Shenzhen Institutes of Advanced Technology
Chinese Academy of Sciences
Shenzhen 518055, China
E-mail: lt.cai@siat.ac.cn

Q. Wan
P. C. Lauterbur, Research Center for Biomedical Imaging
Institute of Biomedical and Health Engineering
Shenzhen Institutes of Advanced Technology
Chinese Academy of Sciences
Shenzhen 518055, China

DOI: 10.1002/adfm.201304225

coordinating solvents.[16] They provide NCs that are dispersible mainly in hydrophobic solutions. Surface chemistry of the NCs is of fundamental importance for biomedical applications. Important criteria for an ideal surface coating include 1) high-affinity for the NCs surface, 2) long-term stability across a broad range of pH and ionic strengths, 3) effective and controllable surface functionalization, 4) minimization of hydrodynamic size, and 5) biocompatibility (nontoxic/nonimmunogenic) with low nonspecific binding. Lots of literatures have focused on improvements to the surface chemistry of the NCs, and it has proved extremely challenging to achieve each of these characteristics simultaneously. Recently, multidentate polymer ligands (using thiol/imidazole as QD-coordinating groups) have been proposed to obtain biocompatible hydrophilic QDs with small hydrodynamic radius and improved stability.[17] However, these excellent polymer ligands have been not yet applied to surface chemistry of QRs.

Since Bawendi and Nie groups have shown the use of QDs for biological in vivo imaging in 2004,[18] it has been attracting significant interest over the past decade.[6c,11b,d,19] Most importantly, careful design of the architecture of QDs enables the creation of nanoprobes that are compatible with several imaging techniques—so-called multimodal imaging. In particular, optical imaging and magnetic resonance imaging (MRI) techniques can be used in a complementary fashion by introducing nanoprobes that exhibit both fluorescent and paramagnetic properties. This is a powerful combination as MRI offers the ability to follow the distribution of molecules in vivo or provide an anatomical reference, whereas optical imaging can be applied to obtain detailed information at subcellular levels. There have been two main ways to assemble different functional building blocks into one multifunctional system. On one hand, it can be directly assembled in a bottom-up approach such as Mn-doped ZnS QDs, Ni-doped CdSeTe QDs.[20] On the other hand, the more promising and versatile strategy is to combine several functional building blocks in a carrier matrix.[21]

In this report, we engineered the synthesis of CdSe-based alloy QRs ($CdTe_xSe_{1-x}$) with high photoluminescence quantum yields (PLQY) and tunable emission. ZnS shells grew on the $CdTe_xSe_{1-x}$ core to enhance the stability. For potential biological applications, the polymer rich in imidazole groups along the backbone was used for QRs water solubilization. For the advantage of combing optical imaging and MRI, paramagnetic Gd^{3+}, MRI contrast agent that is commercial available and clinical implementary, was then conjugated to the surface of QRs by the interaction between metal ions and the high-density ligands to produce dual-modal QRs. The dual modal nanostructure was applied for in vivo fluorescence and magnetic resonance lymph node imaging. Moreover, other functional ions may also be assembled with the QRs, through which a potential nano-platform for designing multifunctional nanostructure was supplied.

2. Results and Discussion

2.1. QRs Synthesis and Characterization

Synthesis of core $CdTe_xSe_{1-x}$ quantum rods was achieved in organic solvent at fixed injection conditions. Typically, $Cd(Ac)_2 \cdot 2.5H_2O$ salts and Tetradecylphosphonic acid (TDPA) were solubilized in trioctylphosphine Oxide (TOPO), the selenium (Se) and tellurium (Te) precursor mixture was injected at 340 °C, stirring for 6 min at 320 °C. To monitor the effect of the composition, all samples with different Te ratios were conducted under the same reaction conditions and transmission electron microscopy (TEM) measurements were carried out. The as-prepared nanocrystals displayed a nearly rod shape with lateral length decreasing from 13.3 ± 1 nm (**Figure 1**a), 12.1 ± 1 nm (Figure 1b), 12.0 ± 1nm (Figure 1c) to 10.8 ± 1 nm (Figure 1d) as Te content increasing. The high-resolution TEM images (Figure 1e–h) of the QRs revealed that a uniform rod shape was obtained with well-resolved lattice fringes, demonstrating the highly crystalline nature of the as-prepared QRs. The photoluminescence (PL) spectra of the QRs were investigated (Figure 1i). It can be observed that the PL spectra shifted from visible to near-infrared region with the increasing of Te ratio. The red-shift of PL emission can be attributed to the narrow band gap of CdTe (1.48 eV), which would tune the emission of CdSe by the formation of alloy or Type-II core-shell structure. The concept has already been applied to synthesis QDs.[14] Therefore, the results demonstrated that the emission of QRs could be tuned by changing the composition. Interestingly, the composition-tunable QRs have a maximum emission with Te ratio at a value of 0.50 (shown in Table S1, Supporting Information). It illustrated that an obvious nonlinear relationship was obtained between composition and bandgap, exhibiting a notable bandgap bowing. It was consistent with the results of the alloyed $CdSe_xTe_{1-x}$ QDs which have been reported previously.[22] X-ray diffraction (XRD) was utilized to confirm the crystalline structure of the QRs. As shown in Figure 1j, the crystal structure of CdSe QRs can be assigned as a typical wurtzite structure with the existence of strong characteristic (002), (102), (110), (103), and (112) peaks. The diffraction peaks of $CdTe_xSe_{1-x}$ QRs gradually shifted to smaller angles with the increasing of Te content. The continuous peak shifting of the QRs also indicated that there was no phase separation or isolated nucleation of CdTe or CdSe in the $CdTe_xSe_{1-x}$ QRs. It was noted that the spectra of core/shell NCs were intermediate between core and shell. Batches of QRs were grown to large size, with the periodic removal of aliquots of the growing QRs in order to confirm their homogeneity. The aliquots were then washed and analyzed by inductively coupled plasma optimal emission spectrometry (ICP-OES). As demonstrated in Figure 1k, the composition remained nearly constant during growth period. This set of elemental data provided strong evidence that the ternary QRs had a homogeneous alloy structure from start to the end of particle growth. We analyzed the concentrations of Te in the alloyed $CdTe_xSe_{1-x}$ QRs and compared them with the initial precursor concentrations (Table S1, Supporting Information). The composition of the alloyed $CdTe_xSe_{1-x}$ QRs consisted of 15% Te as Se was nineteen times of Te in injected precursor solution. Precursor solutions containing Se nine times of Te produced alloyed QRs with 25% Te after nucleation. Similarly, equimolar Te and Se content alloyed $CdTe_xSe_{1-x}$ QRs was obtained containing 20% Te by injecting precursor solutions. These results suggested that TOP-Te reacted much faster with Cd relative to TOP-Se. It was reported that the diatomic bond dissociation energies were 364 kJ mol^{-1} and 298 kJ mol^{-1},

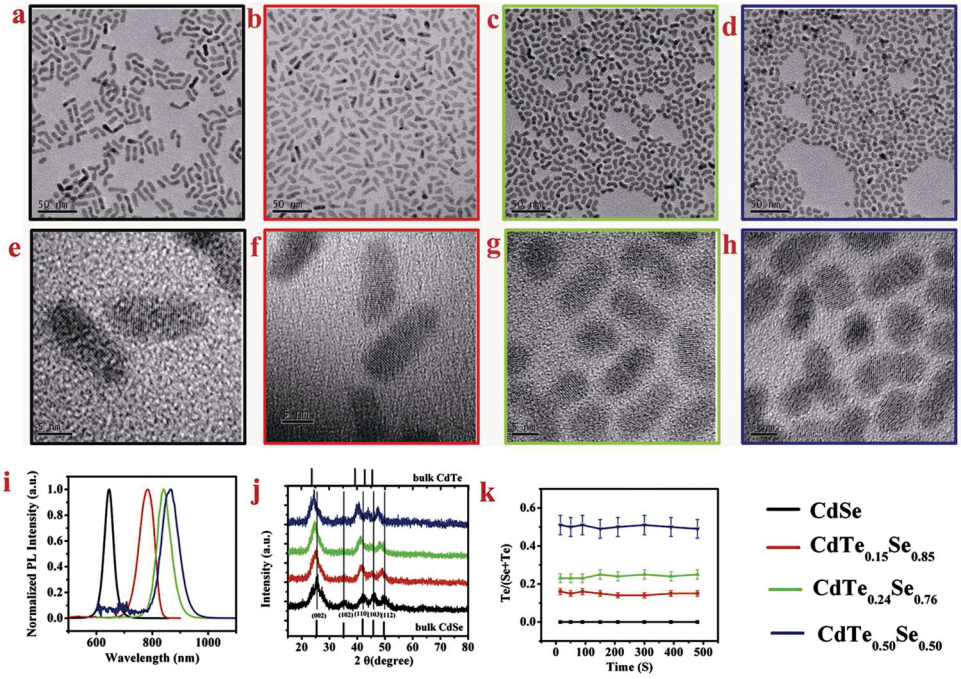

Figure 1. The characterization of $CdTe_xSe_{1-x}$ quantum rods (QRs). a–d) TEM, e–h) HRTEM images, i) PL spectra, j) X-ray power diffraction data and k) plot of particle composition (measured by inductively coupled plasma optimal emission spectrometry) versus time of different samples of $CdTe_xSe_{1-x}$ quantum rods: a) $x = 0$, b) $x = 0.15$, c) $x = 0.24$, d) $x = 0.5$.

respectively between phosphorus and the chalcogen atoms for TOP-Se complex and TOP-Te at room temperature.[23] Obviously, TOP-Te had faster cleavage rate than that of TOP-Se, resulting in a faster reaction rate of the Te with Cd compared to Se. Therefore, homogeneous alloyed QRs were synthesized under the condition of an excess of Se which could satisfy the counterbalance of Te with higher reactivity.

The optical properties of the QRs were not only composition-dependent, but also size-dependent. UV-vis absorption and photoluminescence (PL) spectra were effective techniques for monitoring the growth processes of alloyed QRs. **Figure 2**a showed the temporal evolution of UV-vis absorption and PL emission spectra of the $CdTe_{0.15}Se_{0.85}$ QRs under growth temperature of 300 °C. As the reaction was prolonged from 0.5 to 6 min, its absorption spectra shifted rapidly to longer wavelengths and the absorption peaks that existed in the initial growth stage became weaken as the reaction proceeded. Figure 2b displayed the variation of the PL spectra of $CdTe_{0.15}Se_{0.85}$ QRs with reaction time. The emission peak dramatically shifted from 675 nm to 795 nm. The results indicated that size confinement could partially affect the alloyed QRs. Besides UV-vis absorption and PL emission spectra variation of the QRs, the PL QY of the as-synthesized $CdTe_{0.15}Se_{0.85}$ QRs was plotted in Figure 2c. During the growth process, the PL QY of the as-prepared QRs increased monotonically in the early stage and then gradually decreased as reaching a maximum (≈80%). TEM images of the QRs at different time intervals were also displayed in Figure S1, Supporting Information. It indicated that the monodispersity and particle size of the QRs increased with reaction time.

This rapid and simple synthetic method provided relatively bright (PLQY 40–80%) and near-infrared (650–870 nm) QRs. However, these core-only QRs lost their PL rapidly if the original oil-dispersible QRs were transferred into aqueous media through ligand replacement. The instability of the PL rendered these QRs unsuitable for practical applications. The reason for PL instability of QRs in aqueous media may be due to their intrinsic band offset, which made the electrons to be exposed directly, thus it could be easily captured by the molecules in the solution system. It has been proven that surface passivation of NCs using suitable inorganic materials with a high bandgap was an essential step to enhance PL efficiency and stability.[12a,b,24] Herein, several monolayers (MLs) of ZnS shell were grown

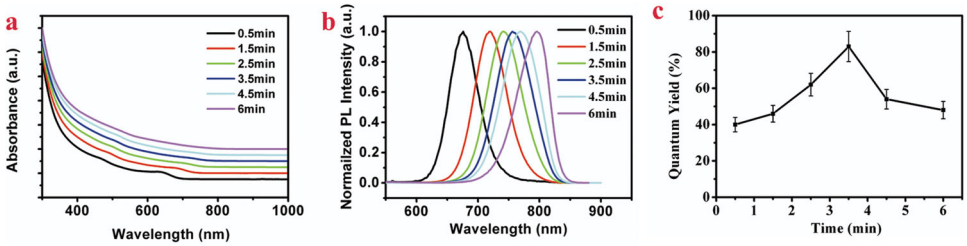

Figure 2. a) UV-vis absorption, b) PL emission spectra, and c) PLQY of the $CdTe_{0.15}Se_{0.85}$ QRs under different growth times.

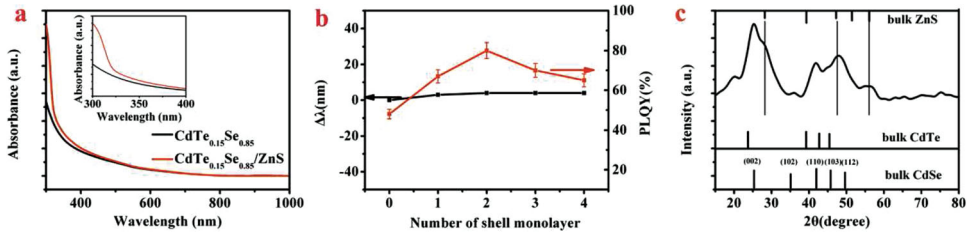

Figure 3. a) Comparison of absorption spectra of $CdTe_{0.15}Se_{0.85}$ and $CdTe_{0.15}Se_{0.85}$/ZnS QRs (inset shows the absorption spectra of core and core/shell QRs between 300–400nm); b) $\Delta\lambda$ ($\lambda_{\text{core-shell emisssion}}-\lambda_{\text{core emission}}$) and PLQY of the QRs with different shell thicknesses; c) XRD of the $CdTe_{0.15}Se_{0.85}$/ZnS QRs.

around the surface of $CdTe_xSe_{1-x}$ QRs to improve their PL stability. As shown in **Figure 3**a, noticeable change in the spectra was the evolution of a broad absorption in the ultraviolet with the addition of Zn/S precursor, which can be ascribed to the formation of the ZnS shell.[24] Upon the ZnS shell growth, no substantial change was observed in the PL emission spectra ($\Delta\lambda$ around 0 nm). The PL QY of the $CdTe_xSe_{1-x}$/ZnS QRs increased significantly (Figure 3b). It could be attributed to the thin shell grown onto QRs surface. However, further layered ZnS shell growth would cause a dramatically PL QY decline. Such behavior was also observed previously for spherical core/shell NCs, which was most likely attributed to the lattice mismatch.[24] While in a thin shell the strain was accommodated, further shell growth leaded to defect formation that can lead to creation of traps. XRD of the $CdTe_xSe_{1-x}$/ZnS QRs was further conducted to confirm the core-shell structure. Peaks of ZnS can be seen in Figure 3c, which further identified the shell of ZnS were formed.[25]

2.2. Surface Modification of QRs

$CdTe_{0.15}Se_{0.85}$/ZnS QRs were chosen to carry out the following experiments for their adequate emission which were not only in the range of near infrared region, but also can be sensitively detected by small animal imaging instrument. Schematic representation of the QRs with images of the organic and aqueous dispersions was shown in **Figure 4**. It indicated that ligand exchange of QRs (capped with the native oleylamine) can be implemented using multidentate polymers with imidazole pendant groups (PMAH, binding with the Zn rich surface of nanorods through the nitrogen of the imidazole) following the protocol reported by our group previously and elsewhere.[17c] And then, the hydrodynamic size of the QRs was measured by dynamic light scattering (DLS). As displayed in Figure 4, the diameter of oleylamine-capped QRs dispersed in chloroform was 12.56 nm, and it slightly increased to 16.47 nm after ligand exchange. It illustrated that these QRs were transferred into aqueous solution without aggregation. Upon ligand exchange with PMAH, the QRs aqueous solutions exhibited identical absorption and PL emission spectral profiles compared to those of initial hydrophobic QRs dispersions in chloroform. The stability of the as-prepared water-soluble QRs was investigated to explore certain potential biological applications. Under irradiation of light at 400 nm for about 2 h, the PMAH-QRs exhibited excellent photo-stability. As shown in Figure S2 (Supporting Information), the PL intensity of QRs increased more than 50% after 30 min illumination and the enhanced fluorescence was retained for about 2 h. This photo-induced fluorescence enhancement phenomenon was attributed to the both contributions of surface passivation by photo-induced charged carriers and the formation of neutral core/charged shell QR states, which has already been studied.[26] Furthermore, the PL intensity of PMAH-QRs was not changed significantly (Figure S3, Supporting Information) after storage under ambient condition for nearly two months.

Previous studies have been shown that the NCs coated with imidazole groups stayed stable in buffers over a range of pH 6–11. Nonetheless, it should be pointed out that the binding of PMAH to the surface of NCs would be disrupted below pH

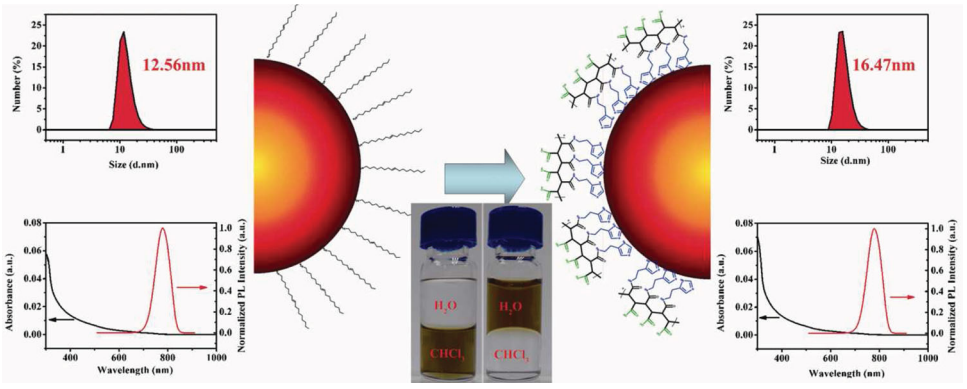

Figure 4. Diameters measured by dynamic light scatting, UV-vis absorption and PL emission spectra of $CdTe_{0.15}Se_{0.85}$/ZnS QRs before (left) and after (right) ligand exchange with PMAH. Schematic representation of the QRs with images of the organic and aqueous dispersions was shown.

5 due to the protonation of imidazole groups, which limited their further biomedical applications. As a result, it has almost become a requirement to incorporate poly(ethylene glycol) (PEG) chains into the surface coatings not only to further enhance the stability but also to reduce nonspecific binding.[27] As shown in **Figure 5**a, PEG was conjugated to the surface of QRs via strain-promoted click chemistry which was ideal for QRs bioconjugation since no addition reagents introduced. The diameters of the QRs coated with PEG with different molecular weight were measured by DLS. The hydrodynamic diameter was 18.08 nm for PEG500-PMAH-QRs, 20.6 nm for PEG1000-PMAH-QRs, and 25.12 nm for PEG2000-PMAH-QRs respectively. Compared to the size of PMAH-QRs (16.47 nm), the sizes of PEGylated QRs were raised with the increase of PEG molecular weight (Figure 5b). ^{1}HNMR spectroscopy of PMAH-QRs and PEGylated PMAH-QRs was also carried out to confirm the existence of PEG on the nanoparticles (Figure S4, Supporting Information). And then, pH stability of the PEGylated QRs was studied (Figure 5c). All of the QRs were stable between pH 7-10. However, QRs were aggregated under pH 4 except the PEG2000-PMAH-QRs. Although at low pH values, the PMAH were protonated and no longer conferring to colloidal stability to the QRs, PEG shielded the QRs against aggregation under harsh pH conditions (pH below 5). Furthermore, we investigated the tolerance of the QRs against ion strength by adding salts. As can be seen in Figure 5d, there was no precipitation of QRs under high concentration of NaCl solution (2 mol L^{-1}), all of the QRs appeared to be resistant to high ion strength. Besides colloidal stability, the fluorescence stability of PEGylated QRs was also investigated (Supporting Information Figure S5,S6). The fluorescence intensity of PEGylated QRs was very stable in the presence of added excess salt with only minor relative intensity changes at pH 5, which is consistent with previous studies.[17d] To test the nonspecific binding of PEGylated QRs, we incubated MCF-7 cells with QRs and subsequently washed the cells using phosphate-buffered saline (PBS). As shown in Figure S7, PMAH-QRs showed very high nonspecific cellular binding and decreased signals have been found in PEG500-PMAH-QRs and PEG1000-PMAH-QRs. In contrast, there was no detectable nonspecific binding for PEG2000-PMAH-QRs at similar concentrations. These results indicated the level of nonspecific binding was inherently low for such PEGylated QRs.

2.3. Construction of Multifunctional Nanostructure for In Vivo Imaging

We engineered a dual-modal imaging nanosystem for fluorescence and magnetic resonance (MR) imaging by adsorbing paramagnetic Gd^{3+} (**Figure 6**a). There were abundant carboxyl groups on the surface of water-soluble QRs, thus Gd^{3+} as positively charged metal ions were conjugated to QRs with negative charges by electrostatic interactions.[28] The stable adsorption of Gd^{2+} was validated by using an ultrafiltration device with a cutoff of 50 kDa and analyzing by ICP-OES (Table S2, Supporting Information). The PEG layer, coupled by click chemistry, protected and stabilized the adsorbed metal ions by steric shielding. Furthermore, it achieved to protect QRs against metal-induced colloid aggregation (Figure 6b). There is no

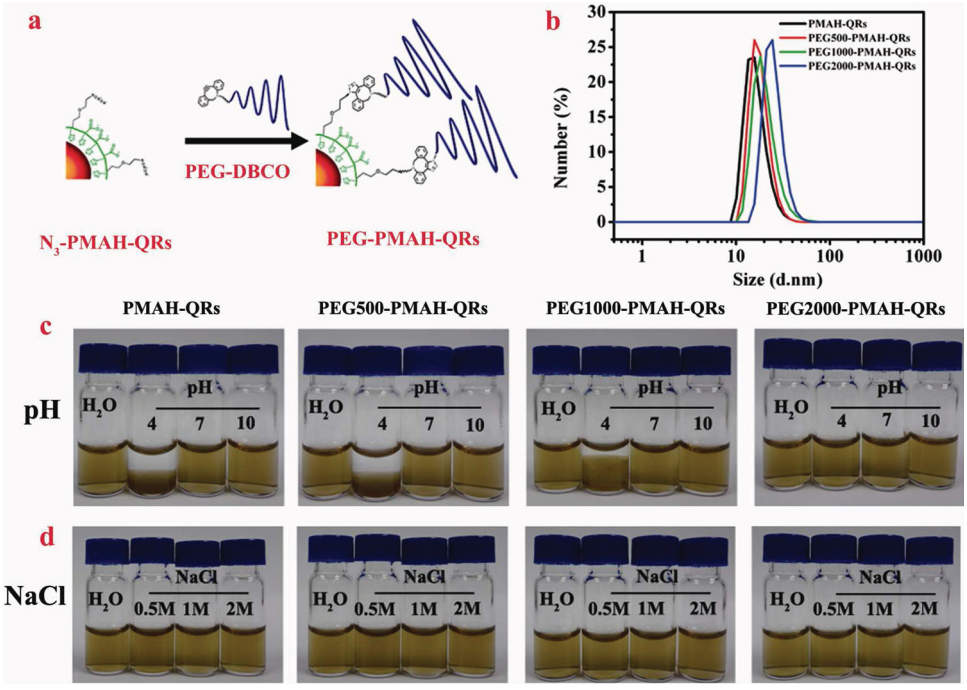

Figure 5. a) Schematic illustration of the conjugation of alkyne-functionalized PEG to azide-functionalized QRs via strain-promoted metal-free click chemistry. b) Hydrodynamic sizes of water-soluble QRs coated with PMAH (PMAH-QRs, 16.47 nm, black) and PEG with different molecular weight (PEG500-PMAH-QRs, 18.08 nm, red; PEG1000-PMAH-QRs, 20.6 nm, green; PEG2000-PMAH-QRs, 25.12 nm, blue) obtained from DLS. Stability test of the water-soluble $CdTe_{0.15}Se_{0.85}$/ZnS QRs dispersed at c) different pH values and d) in various concentration of NaCl solution.

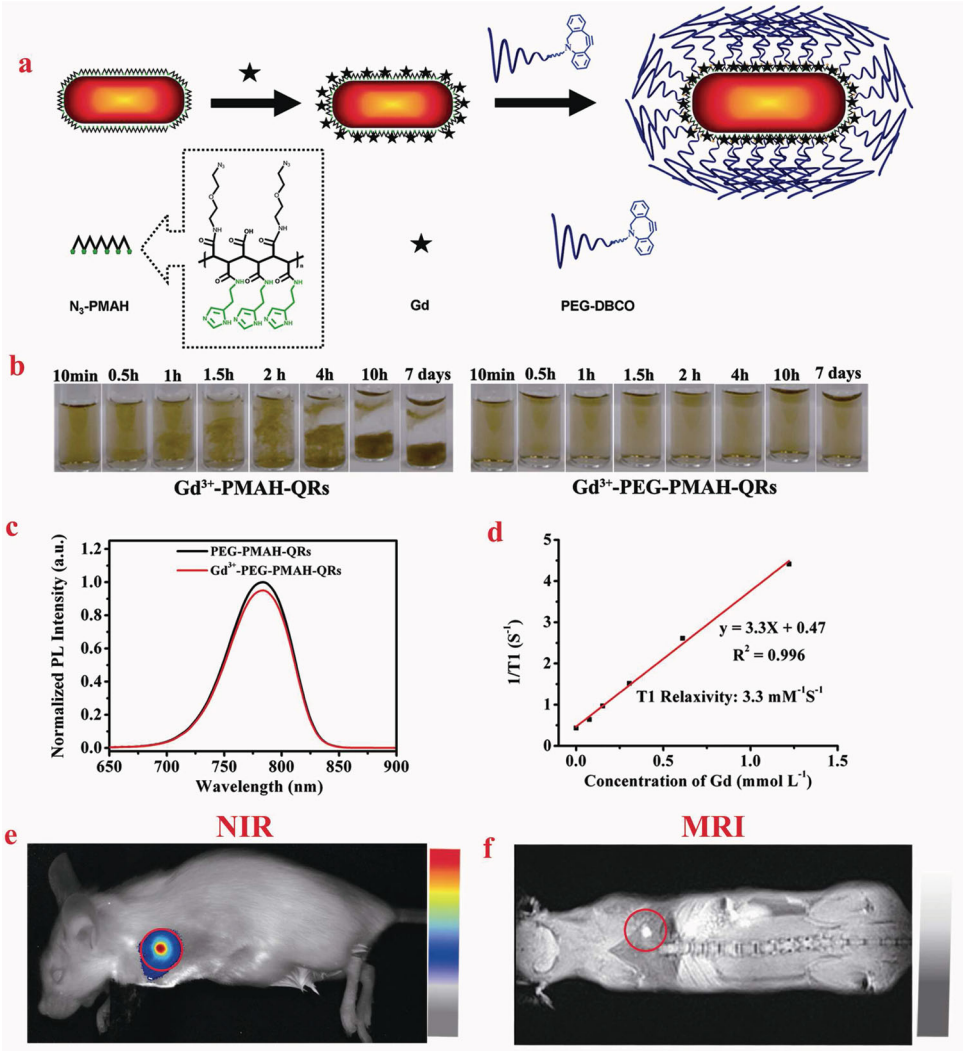

Figure 6. a) Schematic illustration of the preparation of Gd^{3+} functionalized QRs. b) Comparison of store stability between Gd^{3+}-PMAH-QRs and Gd^{3+}-PEG-PMAH-QRs. c) Spectra of the QRs before and after Gd^{3+} conjugation. d) Plot of 1/T1 (s^{-1}) as a function of Gd^{3+} concentration for Gd^{3+}-functionalized CdTeSe/ZnS QRs. The slope indicated the specific relaxivity (3.3 $mM^{-1}S^{-1}$). e) in vivo NIR fluorescence imaging of mouse injected with 0.02 mL (10 mg mL^{-1}) Gd^{3+} -functionalized CdTeSe/ZnS QRs. f) T1 weighted MRI of the mouse. Red circle indicate the lymph node.

obvious change in the emission spectra of QRs before and after Gd^{3+} conjugation (Figure 6c and Figure S8, Supporting Information). The results demonstrated that the fluorescent QRs showed emission peaks at 780 nm and could be easily separated from autofluorescence (Figure S9, Supporting Information). Magnetic resonance imaging capabilities of QRs in water were detected. T1-weighted images in Figure S10 (Supporting Information) clearly exhibited the enhanced MR signal intensities. The R1 (1/T1) relaxivity at different concentrations (0, 0.07, 0.14, 0.29, 0.57, 0.72, 0.86, 1.2, and 1.4 mM) of Gd^{3+} containing nanoparticles was measured, and plotted against the concentration. The R1 was determined from the slope of the linear plot of 1/T1 versus Gd concentration (Figure 6d). From the plot, we obtained the specific relaxivity was 3.3 mM^{-1} S^{-1}. This relaxivity value was close to that of commerial contrast agents such as Magnevist (3.2), Gadovist (3.2), Prohance (2.8), Dotarem (2.8), Omniscan (3.3), and Resovist (2.8). The relaxivity appeared to be higher than that of Teslascan (1.6) and Feridex (2.3), as reported by Rohrer et al.[29] This result illustrated that Gd^{3+} functionalized PEG2000-PMAH-QRs would have significant potential applications as a contrast agent in MRI.

To determine whether PEGylated QRs could be used for in vivo fluorescence and MR imaging, the water-soluble QRs with a concentration of 10 mg mL^{-1} was injected subcutaneously into the distal part of the right anterior paw of healthy mice for regional lymph node mapping. NIR fluorescence imaging was performed using the Maestro in vivo optical imaging system (excitation, 435–480 nm; emission, 490 nm long-pass, 100 ms integration time). The pure autofluorescence spectra and QRs spectra were manually selected from the spectral image of the mice subcutaneously injected with QRs. QRs traveled through the lymphatic and migrated to an axillary location, which indicated the position of lymph node (Figure 6e). It was in accordance with MRI results, which obtained by a clinical 3 Tesla horizontal bore magnet (SIEMENS, VERIO) and demonstrated a dramatically increase signal comparably (Figure 6f, Figure S11,

Supporting Information). In addition, cytotoxicity of the multifunctional QRs were also studied. As shown in Figure S12 (Supporting Information), there was no significant change in cell proliferation for as-prepared QRs (200 μg mL^{-1} QRs highest concentration tested) relative to the control. The results indicated Gd^{3+}-functionalized PEG2000-PMAH-QRs could be used as excellent dual-modal nanoprobes for fluorescence and MR imaging and further explored for engineering multifunction QRs-based nanosystem.

3. Conclusion

In conclusion, we have reported the synthesis of homogeneous alloyed $CdTe_xSe_{1-x}$ QRs with NIR-emitting, which exhibited composition-dependent and size-dependent optical properties. Besides, the rod shape was also composition-tunable. It illustrated that Se played an important role on the shape of nanocrystals, while Te had a significant impact on emitting of that. ZnS shell grown over the $CdTe_xSe_{1-x}$ QRs leaded to high PLQY which was up to over 80% for dispersion in chloroform. Furthermore, cap exchange with PMAH provided $CdTe_xSe_{1-x}$/ZnS QRs that were stable under irradiation of light at 400 nm for about two hours and storage under ambient condition for nearly two months. Colloidal stability was dramatically improved after conjugation of PEG layer by click chemistry. We exhibited that functional metal ions can be introduced into water-soluble $CdTe_xSe_{1-x}$/ZnS QRs. In particular, Gd^{3+} was coupled to the QRs, which opened up the possibility to engineer multifunctional QRs-based nanostructure. We also measured the PL and MRI contrast properties of the Gd^{3+}-functionalized $CdTe_xSe_{1-x}$/ZnS QRs and found that it can be used for in vivo fluorescence and MR imaging. We expected that this approach can be triggered to prepare other nanostructure, which would allow the QRs to be as a nano-platform for novel multifunctional nanostructure.

4. Experimental Section

Materials: Tellurium powder (Te, 99.8%), selenium shot (Se, 99.5%), tri-*n*-octylphosphine oxide (TOPO, 90%), Zinc diethyldithiocarbamate ($Zn(DDTC)_2$, 97%), 1-octadecene (ODE, 90%) and indocyanine green (ICG) standards were purchased from Sigma. Tetradecylphosphonic acid (TDPA, 97%), trioctylphosphine (TOP, 97%) were obtained from Strem Chemicals. Cadmium acetate dehydrate ($Cd(OOCCH_3)_2{\cdot}2H_2O$, 98%) was purchased from Alfa Aesar. Oleylamine (OAm, 90%) was from Acros Organics. Poly (maleic anhydride) (MW = 5000 Da) was purchased from PolySciences, Inc, USA. PEG was obtained from Biomatrik Inc., China. DBCO-NHS ester was purchased from Click Chemistry Tools (Scottsdale, FL, USA). All other chemicals used in this study were of analytical reagent grade and used without further purification. Ultrapure water (18.25 MΩ cm, 25 °C) was used in all experiments.

Synthesis of Alloyed $CdTe_xSe_{1-x}$ and $CdTe_xSe_{1-x}$ /ZnS Quantum Rods: A selenium stock solution (1 M) was prepared by dissolving 0.79 g of selenium shot in 10 mL of TOP, yielding a colorless solution. A tellurium stock solution at the same concentration was prepared by dissolving 1.28 g of tellurium powder in 10 mL of TOP, yielding a yellow saturated solution. To obtain the alloyed QRs, 0.5 g of TDPA, 5 g of TOPO, and 0.26g of Cd $(OOCCH_3)_2{\cdot}2H_2O$ was heated to 100 °C and was degassed under a vacuum of 20 Pa for 30 min. The flask was then filled with argon gas, and its temperature was increased to 350 °C. After the precursor Cd was dissolved completely in the solvent, the temperature was lowered to 340 °C and was allowed to stabilize for several minutes. For convenient control of reagent molar ratios, seven premixed Se and Te solutions were prepared from the individual stock solutions at 1 M total concentration, but with Te: (Te + Se) molar ratios of 0, 0.05, 0.1, 0.2, 0.4, 0.8, or 1. The premixed solution was rapidly injected into the colorless Cd solution at 340 °C. Aliquots of the reaction mixture were taken and quenched in cold (25 °C) chloroform. The as-prepared $CdTe_xSe_{1-x}$ QRs were isolated through precipitation from excess acetone, and then dissolved in hexane. The solution of $CdTe_xSe_{1-x}$ was diluted in a mixture of trioctylphosphine oxide (5 g), and Oleylamine, and hexane was removed under vacuum at 60 °C. The solution was further evacuated for at least 30 min at 100 °C and purged with argon. After heating to 130 °C, a ZnS shell was grown on the QRs using dropwise injection of a solution of 0.1 M $Zn(DDTC)_2$. The QRs were annealed at 180 °C for 20 minutes to allow the growth of the first ZnS monolayer. Next, the temperature of the reaction solution was allowed to decrease to 130 °C, and then, 3 mL of $Zn(DDTC)_2$ precursor solution was added to the reaction flask for the growth of the second monolayer of ZnS shell. For the third, the temperature cycling was continued by injecting 5 mL of the single precursor $Zn(DDTC)_2$ solutions. When the desired synthesis was completed, the reaction was cooled down to room temperature and isolated through precipitation from excess ethanol.

QRs Structural and Compositional Characterization: Ultraviolet–visible (UV-vis) absorbance spectra were taken using a PerkinElmer Lambda 25 UV-Vis absorption spectrophotometer. Photoluminescence (PL) spectra were recorded with an Edinburgh F900 fluorescent spectrometer. Transmission electron microscopy (TEM) and High-resolution Transmission electron microscopy (HRTEM) images were taken on a FEI Tecnai G20 transmission microscope at 200 kV. Samples for TEM observation were prepared through dropped 10 μL of the solution on a carbon-coated grid and allowed the sample to dry. X-ray diffraction patterns were acquired using a Philips X'Pert diffractometer with a Cu Kα source. Inductively coupled plasma optimal emission spectrometry (ICP-OES) was used to measure the contents of the QRs. Photoluminescence quantum yields were measured using indocyanine green (ICG) as a standard (13.2% in DMSO). The QYs were obtained following

$$QY_{QRs} = QY_{dye}\frac{I_{QRs}}{I_{dye}}\frac{A_{dye}}{A_{QRs}}\frac{n_{QRs}^2}{n_{dye}^2}$$

Where $n_{QRs,dye}$ is the refractive index, $A_{QRs,dye}$ is the absorption, and $I_{QRs,dye}$ is the integrated fluorescence signal for the QRs and dye solutions, respectively.

Multidentate Polymer Ligand Synthesis: Imidazole-based multidentate polymer was synthesized according previously reported method. Briefly, 100 mg of poly(maleic anhydride) (MW = 5000 Da) was dissolved in 5 mL of DMSO containing 20 mg of DMAP, and 120 mg of histamine was added as solid. With the reaction going on at room temperature, the histamine solid gradually dissolved within 2 h. After another 4 h, the product, named as PMAH, was purified by precipitation in water followed by lyophilization. The obtained product has excellent solubility in strongly polar solvents (such as DMSO, DMF or water). To synthesize the azido-derivatized multidentate polymer (N_3-PMAH), a mixture of histamine and N_3-PEG-NH_2 was used instead of pure histamine.

QRs Solubilization in Water: The core-shell QRs were transfer into water by ligand exchange that reported previously by our group. In a typical procedure, organic-soluble QRs were dispersed in chloroform. The QRs stock solution was mixed with PMAH (or N_3-PMAH) solution of DMSO, and stirred for 10 min at RT, after which TMAOH was added and stirred for an additional 20 min to form a biphasic system. The solution was centrifuged at 5000*g* for 10 min to achieve phase separation. The organic layer was removed by pipette and any residual chloroform was removed from the aqueous phase by evaporation with stirring under reduced pressure. The PMAH (or N_3-PMAH) coated QRs were precipitated by centrifugation twice with the addition of acetone and redispersed in PBS buffer at pH 7.4. Free unbound PMAH (or N_3-PMAH) ligands were removed by an ultrafiltration device with a cutoff of 50 kDa (Millipore).

Preparation of PEGylated QRs by Click Chemistry: Firstly, the dibenzocyclooctyne (DBCO, a strained cyclooctyne moiety) was linked to the end of amino-PEG. The PEG was incubated with DBCO-NHS ester (Click Chemistry Tools) for 2 h at room temperature. Unbound DBCO-NHS ester was removed by precipitation in water followed by lyophilization. And then, azido-derivatized QRs and PEG-DBCO were mixed in 1× PBS with and incubated for 2 hrs at 37 °C. Unreacted PEG was removed by an ultrafiltration device with a cutoff of 50 kDa (Millipore).

Preparation of PEGylated Multimodal QRs: A freshly prepared Gd^{3+} solution was added dropwise to rapidly mixing QRs, which facilitated even distributions of the Gd^{3+} on the surface of QRs. After 10 min, PEG-DBCO were added and incubated for 2 h at 37 °C. Unreacted PEG was removed by an ultrafiltration device with a cutoff of 50 kDa (Millipore).

Cell Culture: MCF-7 cells (human breast cancer cells) were cultured in Dulbecco's Modified Eagle Medium (DMEM, HyClone) supplemented with 10% (v/v) fetal bovine serum, 1% (v/v) penicillin, and 1% (v/v) streptomycin. Cells were incubated in a humidified incubator at 37 °C with 5% CO_2.

Animals: Six- to 8-week-old Balb/c mice were obtained from Guangdong Province Laboratory Animal Center (Guangzhou, China), and maintained in the institutional animal care facility. The mice were acclimated for 1 week prior to use. All animal protocols were approved by Institutional Animal Care and Usage Committee of Shenzhen Institutes of Advanced Technology.

In Vitro MR Imaging: The relaxation times at low field strength were measured on a 0.55 T MRI instrument (MicroMRI, Shanghai Niumag Corp.) at 32 °C. A quadrature coil with an inner diameter of 1.8 cm was used for RF transmission and reception. For T1 measurements, samples with various Gd^{3+} concentrations (determined by ICP-OES) were dispersed in water. T1 measurements were performed using an inversion recovery (IR) sequence with various inversion times (TI). The experimental parameters were as follows: FOVRead = 80 mm, FOVPhase = 80 mm, TR = 200 ms, TE = 10 ms, Slice Width = 6.0 mm, Slice Gap = 0.5 mm. It has been added to the revised supporting information.

In Vivo Dual Modal Imaging: In vivo optical imaging was carried out using a Maestro GNIR Flex imaging system (CRi) along with image acquisition and analysis software from CRi. When the tunable liquid crystal filter in the Nuance GNIR CCD camera (Cambridge Research & Instrumentation Inc., CRi) was stepped by an increment of 10 nm from 650 to 950 nm, the whole-body image of a mouse was captured with a constant exposure time at each step. The orange excitation was performed for imaging. MRI experiments were performed on a clinical 3 Tesla horizontal bore magnet (SIEMENS, VERIO). The pulse sequence time parameters (TE/TR) of T1 weighted imaging were as follows: TE = 9 ms, TR = 500 ms.

Supporting Information

Supporting Information is available from the Wiley Online Library or from the author.

Acknowledgements

D.G. and P.F.Z. contributed equally to this work. This work was supported by the National Basic Research Program of China (973 Program No. 2011CB933600), the National Natural Science Foundation of China (Grant No. 81071249 and 20905050), the Science and Technology Foundation of Guangdong Province of China (Grant No. 2009A030301010, and 9478922035-X003399), Guangdong Innovation Reasearch Team of Low-cost Healthcare and Shenzhen Science and Technology Program (Grant No. JC201005260247A, CXB201005250029A).

Received: December 19, 2013
Revised: February 2, 2014
Published online: April 1, 2014

[1] a) C. A. Morris, M. L. Anderson, R. M. Stroud, C. I. Merzbacher, D. R. Rolison, *Science* **1999**, *284*, 622; b) F. Caruso, *Chem. Europ. J.* **2000**, *6*, 413.
[2] a) J. Kong, N. R. Franklin, C. Zhou, M. G. Chapline, S. Peng, K. Cho, H. J. Dai, *Science* **2000**, *287*, 622; b) D. Y. Zhai, B. Liu, Y. Shi, L. J. Pan, Y. Q. Wang, W. B. Li, R. Zhang, G. H. Yu, *ACS Nano* **2013**, *7*, 3540; c) J. T. Zhang, J. F. Liu, Q. Peng, X. Wang, Y. D. Li, *Chem. Mater.* **2006**, *18*, 867.
[3] a) J. M. Bruchez, M. Moronne, P. Gin, S. Weiss, A. P. Alivisatos, *Science* **1998**, *281*, 2013; b) W. C. W. Chan, S. M. Nie, *Science* **1998**, *281*, 2016; c) J. Xie, F. Zhang, M. Aronova, L. Zhu, X. Lin, Q. Quan, G. Liu, G. F. Zhang, K. Y. Choi, K. Kim, X. L. Sun, S. Lee, S. H. Sun, R. Leapman, X. Y. Chen, *ACS Nano* **2011**, *5*, 3043; d) B. J. Nehilla, P. G. Allen, T. A. Desai, *ACS Nano* **2008**, *2*, 538.
[4] a) W. U Huynh, J. J. Dittmer, A. P. Alivisatos, *Science* **2002**, *295*, 2425; b) V. I. Klimov, A. A. Mikhailovsky, S. Xu, A. Malko, J. A. Hollingsworth, C. A. Leatherdale, H. J. Eisler, M. G. Bawendi, *Science* **2000**, *290*, 314.
[5] a) X. G. Peng, L. Manna, W. D. Yang, J. Wickham, E. Scher, A. Kadavanich, A. P. Alivisatos, *Nature* **2000**, *404*, 59; b) C. J. Murphy, N. R. Jana, *Adv. Mater.* **2002**, *14*, 80; c) M. F. Tsai, G. S. H. Chang, F. Y. Cheng, V. Shanmugam, Y. S. Cheng, C. H. Su, C. S. Yeh, *ACS Nano* **2013**, *7*, 5330; d) W. Li, R. Zamani, P. R. Gil, B. Pelaz, M. Ibáñez, D. Cadavid, A. Shavel, R. A. Alvarez-Puebla, W. J. Parak, J. Arbiol, A. Cabot, *J. Am. Chem. Soc.* **2013**, *135*, 7098.
[6] a) J. T. Hu, L. S. Li, W. D. Yang, L. Manna, L. W. Wang, A. P. Alivisatos, *Science* **2001**, *292*, 2060; b) M. Kazes, D. Y. Lewis, Y. Ebenstein, T. Mokari, U. Banin, *Adv. Mater.* **2002**, *14*, 317; c) S. Deka, A. Quarta, M. G. Lupo, A. Falqui, S. Boninelli, C. Giannini, G. Morello, M. D. Giorgi, G. Lanzani, C. Spinella, R. Cingolani, T. Pellegrino, L. Manna, *J. Am. Chem. Soc.* **2009**, *131*, 2948.
[7] H. Htoon, J. A. Hollingworth, A. V. Malko, R. Dickerson, V. I. Klimov, *Appl. Phys. Lett.* **2003**, *82*, 4776.
[8] A. Shabaev, L. Efros, *Nano Lett.* **2004**, *4*, 1821.
[9] T. Mokari, U. Banin, *Chem. Mater.* **2003**, *15*, 3955.
[10] K. T. Yong, I. Roy, H. E. Pudavar, E. J. Bergey, K. M. Tramposch, M. T. Swihart, P. N. Prasad, *Adv. Mater.* **2008**, *20*, 1412.
[11] a) A. H. Fu, W. W. Gu, B. Boussert, K. Koski, D. Gerion, L. Manna, M. L. Gros, C. A. Larabell, A. P. Alivisatos, *Nano Lett.* **2007**, *7*, 179; b) K. T. Yong, J. Qian, I. Roy, H. H. Lee, E. J. Bergey, K. M. Tramposch, S. He, M. T. Swihart, A. Maitra, P. N. Prasad, *Nano Lett.* **2007**, *7*, 761; c) G. Xu, K. T. Yong, I. Roy, S. D. Mahajan, H. Ding, S. A. Schwartz, P. N. Prasad, *Bioconjugate Chem.* **2008**, *19*, 1179; d) R. Kumar, H. Ding, R. Hu, K. T. Yong, I. Roy, E. J. Bergey, P. N. Prasad, *Chem. Mater.* **2010**, *22*, 2261; e) K. T. Yong, R. Hu, I. Roy, H. Ding, L. A. Vathy, E. J. Bergey, M. Mizuma, A. Maitra, P. N. Prasad, *ACS App. Mat. Interfaces* **2009**, *1*, 710; f) R. Alam, D. M. Fontaine, B. R. Branchini, M. M. Maye, *Nano Lett.* **2012**, *12*, 3251.
[12] a) M. A. Hines, P. Guyot-Sionnest, *J. Phys. Chem.* **1996**, *100*, 468; b) X. G. Peng, M. C. Schlamp, A. V. Kadavanich, A. P. Alivisatos, *J. Am. Chem. Soc.* **1997**, *119*, 7019; c) R. G. Xie, U. Kolb, J. X. Li, T. Basche, A. Mews, *J. Am. Chem. Soc.* **2005**, *127*, 7480.
[13] a) Y. T. Lim, S. Kim, A. Nakayama, N. E. Stott, M. G. Bawendi, J. V. Frangioni, *Mol. Imaging* **2003**, *2*, 50; b) X. Michalet, F. F. Pinaud, L. A. Bentolia, J. M. Tsay, S. Doose, J. J. Li, G. Sundaresan, A. M. Wu, S. S. Gambhir, S. Weiss, *Science* **2005**, *307*, 538.
[14] R. E. Bailey, S. M. Nie, *J. Am. Chem. Soc.* **2003**, *125*, 7100.
[15] L. A. Swafford, L. A. Weigand, M. J. Bowers, J. R. McBride, J. L. Rapaport, T. L. Watt, S. K. Dixit, L. C. Feldman, S. J. Rosenthal, *J. Am. Chem. Soc.* **2006**, *128*, 12299.
[16] a) C. B. Murray, D. J. Norris, M. G. Bawendi, *J. Am. Chem. Soc.* **1993**, *115*, 8706; b) X. G. Peng, *Small* **2002**, *2*, 334; c) S. H. Sun, H. Zeng, *J. Am. Chem. Soc.* **2002**, *124*, 8204.

[17] a) H. B. Na, G. Palui, J. T. Rosenberg, X. Ji, S. C. Grant, H. Mattoussi, *Acs Nano* **2012**, *6*, 389; b) A. M. Smith, S. M. Nie, *J. Am. Chem. Soc.* **2008**, *130*, 11278; c) P. F. Zhang, S. H. Liu, D. Y. Gao, D. H. Hu, P. Gong, Z. H. Sheng, J. Z. Deng, Y. F. Ma, L. T. Cai, *J. Am. Chem. Soc.* **2012**, *20*, 8388; d) W. Liu, A. B. Greytak, J. Lee, C. R. Wong, J. Park, L. F. Marshall, W. Jiang, P. N. Curtin, A. Y. Ting, D. G. Nocera, D. Fukumura, R. K. Jain, M. G. Bawendi, *J. Am. Chem. Soc.* **2010**, *132*, 472.

[18] a) S. Kim, Y. T. Lim, E. G. Soltesz, A. M. De Grand, J. Lee, A. Nakayama, J. A. Parker, T. Mihaljevic, R. G. Laurence, D. M. Dor, L. H. Cohn, M. G. Bawendi, J. V. Frangioni, *Nat. Biotechnol.* **2004**, *22*, 93; b) X. H. Gao, Y. Y. Cui, R. M. Levenson, L. W. K. Chung, S. M. Nie, *Nat. Biotechonl.* **2004**, *22*, 969.

[19] a) F. Erogbogbo, K. T. Yong, I. Roy, R. Hu, W. C. Law, W. W. Zhao, H. Ding, F. Wu, R. Kumar, M. T. Swihart, P. N. Prasad, *Acs Nano* **2011**, *5*, 413; b) T. Pons, E. Pic, N. Lequeux, E. Cassette, L. Bezdetnaya, F. Guillemin, F. Marchal, B. Dubertret, *Acs Nano* **2010**, *4*, 2531; c) Y. P. Gu, R. Cui, Z. L. Zhang, Z. X. Xie, D. W. Pang, *J. Am. Chem. Soc.* **2012**, *134*, 79.

[20] a) N. Singh, S. Charan, K. Sanjiv, S. H. Huang, Y. C. Hsiao, C. W. Kuo, F. C. Chien, T. C. Lee, P. Chen, *Bioconjugate Chem.* **2012**, *23*, 421; b) R. Zeng, M. Rutherford, R. Xie, B. Zou, X. G. Peng, *Chem. Mater.* **2010**, *22*, 2107.

[21] a) C. Alric, J. Taleb, G. Le Duc, C. Mandon, C. Billotey, A. Le Meur-Herland, T. Brochard, F. Vocanson, M. Janier, P. Perriat, S. Roux, O. Tillement, *J. Am. Chem. Soc.* **2008**, *130*, 5908; b) C. P. Tsai, Y. Hung, Y. H. Chou, D. M. Huang, J. K. Hsiao, C. Chang, Y. C. Chen, C. Y. Mou, *Small* **2008**, *4*, 186; c) G. J. Stasiuk, S. Tamang, D. Imbert, C. Poillot, M. Giardiello, C. Tisseyre, E. L. Barbier, P. H. Fries, M. de Waard, P. Reiss, M. Mazzanti, *ACS Nano* **2011**, *5*, 8193.

[22] Y. C. Li, H. Z. Zhong, R. Li, Y. Zhou, C. H. Yang, Y. F. Li, *Adv. Funct. Mater.* **2006**, *16*, 1705.

[23] A. E. Saunders, A. Ghezelbash, P. Stood, B. A. Korgel, *Langmuir* **2008**, *24*, 9043.

[24] B. O. Dabbousi, J. Rodriguez-Viejo, F. V. Mikulec, J. R. Heine, H. Mattoussi, R. Ober, K. F. Jensen, M. G. Bawendi, *J. Phys. Chem. B* **1997**, *101*, 9463.

[25] L. Manna, E. C. Scher, L. S. Li, A. P. Alivisatos, *J. Am. Chem. Soc.* **2002**, *124*, 7136.

[26] C. T. Yuan, W. C. Chou, D. S. Chuu, Y. N. Chen, C. A. Lin, W. H. Chang, *Appl. Phys. Lett.* **2008**, *92*, 183108.

[27] a) S. Pathak, S. K. Choi, N. Arnheim, M. E. Thompson, *J. Am. Chem. Soc.* **2001**, *123*, 4103; b) D. Gerion, W. J. Parak, S. C. Williams, D. Zanchet, C. M. Micheel, A. P. Alivisatos, *J. Am. Chem. Soc.* **2002**, *124*, 7070; c) E. L. Bentzen, I. D. Tomlinson, J. Mason, P. Gresch, M. R. Warnement, D. Wright, E. Sanders-Bush, R. Blakely, S. J. Rosenthal, *Bioconjugate Chem.* **2005**, *16*, 1488; d) H. Duan, S. Nie, *J. Am. Chem. Soc.* **2007**, *129*, 3333; e) X. Wu, H. Liu, J. Liu, K. N. Haley, J. A. Treadway, J. P. Larson, N. Ge, F. Peale, M. P. Bruchez, *Nat. Biotechnol.* **2003**, *21*, 41.

[28] L. R. Hirsch, A. M. Gobin, A. R. Lowery, F. Tam, R. A. Drezek, N. J. Halas, J. L. West, *Ann. Biomed. En.* **2006**, *34*, 15.

[29] M. P. B. Rohrer, H. Bauer, J. Mintorovitch, M. Requardt, H. J. Weinmann, *Invest. Radiol.* **2005**, *40*, 715.